PHYSICAL REVIEW B, VOLUME 64, 125302

Electronic structure consequences of In/Ga composition variations in self-assembled $In_xGa_{1-x}As/GaAs$ alloy quantum dots

J. Shumway, A. J. Williamson, and Alex Zunger
National Renewable Energy Laboratory, Golden, Colorado 80401

A. Passaseo, M. DeGiorgi, and R. Cingolani
Dipartimento Ingegneria dell'Innovazione, Università di Lecce, 73100 Lecce, Italy

M. Catalano
Insituto CNR-IME, c/o Dipartimento Ingegneria dell'Innovazione, Università di Lecce, 73100 Lecce, Italy

P. Crozier
Center for Solid State Science, Arizona State University, Tempe, Arizona 85287-1704

(Received 22 March 2001; published 5 September 2001)

Provided that the shape, size, and composition profile of semiconductor-embedded quantum dots are given, theory is able to accurately calculate the excitonic transitions, including the effects of inhomogeneous strain, alloy fluctuations, electron-hole binding, and multiband and intervalley coupling. While experiment can accurately provide the spectroscopic signature of the excitonic transitions, accurate determination of the size, shape, and composition profile of such dots is still difficult. We show how one can arrive at a consistent picture of both the material and the electronic structure by interactive iteration between theory and experiment. Using high-resolution transmission electron microscopy, electron-energy-loss spectroscopy, and photoluminescence (PL) spectroscopy in conjunction with atomistic empirical pseudopotential calculations, we establish a model consistent with both the observed material structure and measured electronic/optical properties of a quantum dot sample. The structural model with best agreement between measured and predicted PL is a truncated cone with height 35 Å, base diameter 200 Å, and top diameter 160 Å, having a nonuniform, peaked composition profile with average 60% In content. Next, we use our best structure to study the effect of varying (i) the amount of In in the dots, and (ii) the spatial distribution of In within the dots. We find that by either increasing the amount of In within the dot or by concentrating a given amount of In near the center of the dot, both electrons and holes become more strongly bound to the dot. A small change of In content from 50 to 60% causes an exciton redshift of about 70 meV. Changing the composition profile from a uniform In distribution to a centrally peaked distribution can redshift the exciton by an additional 20–40 meV.

DOI: 10.1103/PhysRevB.64.125302 PACS number(s): 78.66.−w, 85.35.Be

I. INTRODUCTION

A. Interdependence of theory and experiment in determining the material and electronic structure of dots

Correct prediction of the excitonic gap of a semiconductor-embedded ''self-assembled'' quantum dot (QD) is highly nontrivial, yet it is a crucial prerequisite for understanding the basic optical properties of such systems. Even if the size, shape, and composition profile were know exactly, an appropriate theory must take into account (i) the existence of strong multiband coupling (e.g., electron-hole, hole-hole) without which the orbital symmetry, polarization ratio, and level splitting pattern can be qualitatively incorrect,[1–3] (ii) the existence of inhomogeneous and possibly anharmonic strain that not only varies strongly from the base to the top of the dot, but also has a lower point-group symmetry than that gleaned from the geometric shape of the dot,[4] (iii) multivalley (e.g., $\Gamma-X$) interactions[5,6] that may localize wave functions at the interface, (iv) the presence of significantly screened and size-dependent direct and exchange Coulomb interactions that shift the excitonic gap,[7,8] and (v) the possibility that the dot and its wetting layer (WL) are a random alloy rather than a pure phase,[9–13] with a possibly nonuniform composition profile,[14–16] necessitating a correct description of alloy statistical fluctuations.[17,18] Pseudopotential models of such quantum dots[1,2,19–21] are capable of taking these effects into account by retaining the atomistic nature of the system. These models use fast ''order N'' diagonalization of the pseudopotential Hamiltonian,[2,22] and are an alternative to the commonly used effective-mass[23–30] and $\mathbf{k}\cdot\mathbf{p}$[32–35] envelope-function approximations.

It has been possible in the past to fit the excitonic gap via models that neglect all, or most, physical factors indicated above.[24,25,27] Indeed, even single-band effective-mass treatments without explicit strain effects have successfully adjusted the geometric and other physical parameters of the dot to fit the measured gap.[24,25,27] However, it is now known that for a *given* size, shape, and composition of a self-assembled dot, simple theoretical models such as single-band effective mass produce significant errors in the excitonic gap and level spacings relative to more complete theoretical models using identical input parameters.[36] For example, assuming a pyramidal InAs dot with a base of 113 Å and height of 56 Å embedded in GaAs, and comparing to a pseudopotential treatment of the same Hamiltonian,[36] a single-band effective-

©2001 The American Physical Society

1.40-eV excitonic gap, in excellent agreement with the observed PL peak at 1.4 eV, as well as the actual WL thickness from TEM. We therefore scale the In/As profiles determined by EDX and EELS so that the maximum of the In/As counts measured in the WL region corresponds to $x_{\mathrm{In}}=$

A. Computing the equilibrium atomic positions

We place the InGaAs/GaAs alloy dot and wetting layer inside a supercell containing GaAs with dimensions $339\times339\times339$ Å (that is, $60a\times60a\times60a$, where $a=5.65$ Å for bulk GaAs) and apply periodic boundary conditions to the supercell. The cell has been chosen to be large enough that interactions between periodic images do not significantly affect the strain fields and electronic wave functions.

Instead of treating strain with harmonic continuum elasticity theory, as is commonly used for dislocation free heterostructures,[28,32] we treat strain with an atomistic valence force field (VFF) model.[4,21,49,50] VFF offers a couple of advantages over harmonic continuum elasticity theory: (i) VFF can capture anharmonic effects, which are important in InAs/GaAs systems with 7% lattice mismatch (see Ref. 51 for a comparison of formation energies as calculated by VFF and first principles), and (ii) unlike contiuum elasticity models that depict conical or lens-shaped dots as having cylindrical symmetry, VFF has the correct point-group symmetry (C_{2v}), arising from the underlying zinc-blende lattice.[4] Our implementation of the VFF includes bond stretching, bond-angle bending, and bond-length/bond-angle interaction terms, so that we have three force constants for each material, which are fit to reproduce the C_{11}, C_{12}, and C_{44} elastic constants of the material.[21] The equilibrium atomic positions are determined by minimizing VFF total energy using a conjugate gradients algorithm. The length of the supercell in the [001] direction must also be relaxed due to expansion of the epitaxially strained InGaAs wetting layer, while the in-plane dimensions are fixed to the lattice constant of the GaAs substrate.

B. Determination of single-particle eigenstates

Having determined the atomic positions, we use a pseudopotential Hamiltonian to model the electronic structure of the dots,

$$H=-\frac{1}{2}\nabla^2+\sum_{\alpha,n} v_\alpha[\mathbf{r}-\mathbf{R}_{\alpha n},\mathrm{Tr}(\boldsymbol{\epsilon}_{\alpha n})]+v_\alpha^{(\mathrm{SO})}, \qquad (1)$$

where α runs over atom species (In, Ga, and As), and n indexes the atoms. The local part of the pseudopotential, v_α, includes dependence on the local hydrostatic strain[19] $\mathrm{Tr}(\boldsymbol{\epsilon})$ and has been fit to bulk properties, including band structures, experimental deformation potentials, experimental effective masses, first-principles calculations of the valence-band offsets of GaAs and InAs, and the alloy bowing parameter of the InGaAs band gap.[21] Spin orbit interactions are included[21] via a nonlocal potential $v_\alpha^{(\mathrm{SO})}$.[21]

We solve the Hamiltonian Eq. (1) for the band-edge eigenstates using the strained linear combination of bulk bands (SLCBB) method.[2] The SLCBB methods has two features: (i) Wave functions are expanded in a basis set chosen from the bulk Bloch orbitals of materials (and strains) characteristic of the inhomogeneous system being solved,

$$\psi(\mathbf{x})=\sum_{n}^{N_B}\sum_{k}^{N_k} C_{n,k}\phi_{n,k}^{0}(\mathbf{x}), \qquad (2)$$

where n indexes a set of bulk bands from different materials in various strain states, and vectors k are chosen from physically important regions of the Brillouin zone, both Γ and off Γ. (In $\mathbf{k}\cdot\mathbf{p}$ only Γ states are used.) This allows a physically motivated basis to be chosen that is much smaller than a plane-wave expansion, and is independent of system size.

this work. Note that these Coulomb energies are are evaluated from atomistic pseudopotential wave functions, not envelope functions.[7]

IV. INTERPLAY OF EXPERIMENT AND THEORY

A. First measurement of size and shape: Model 1

A first rough assessment of the dot shape and size was performed by a combination of atomic force microscopy (AFM) and TEM plan-view images. The former measurement was performed on uncapped quantum dots, showing the uniform dot base size distribution peaked around 150 Å, of height 35 Å. The capped samples were analyzed by TEM plan-view (see top of Fig. 3), showing a truncated pyramidal shape. The profile could not be determined very accurately by the plan view due to the complex image contrast, which is affected by strain, composition, and sample thickness. However, by combining the information obtained by the two methods we determined the structure to be a truncated conical shape, with a base diameter 150 Å, height 35 Å, and top diameter 70 Å.

Position resolved EDX and EELS experiments were performed by scanning a probe with a FWHM smaller than 1 nm both across several dots and across several regions on the wetting layer. The top portion of Fig. 4 is a STEM image of two dots. ''A'' and ''B'' mark respectively the lines where the scans were performed, corresponding to (*A*) a dot and (*B*) the wetting layer far from the dots. The strain contrast around the dot in the STEM image is evident. To check the concentration of In in the well and the dot we carried out position resolved EDX and EELS analysis.

The In/As concentration ratio derived from EELS is plotted as a function of position for the dot (graph ''A'' in Fig. 4) and the wetting layer (graph ''B'' in Fig. 4). The composition profiles derived from EDX (not shown depletion of In from the wetting layer. We model the dot on a 6-ML wetting layer with a 30% In content [see Fig. 1(a)]. For simplicity we neglect the possibility of diffusion of In into the above capping layer. To study the effect of the In distribution, we have varied the In composition, using both a uniform profile and a nonuniform, peaked profile [shown on the left and right sides of Fig. 1(a)]. Based on the available data, we assume that the In concentration changes with height, using a piecewise linear function with a peaked maximum at one-third the dot height.

acters in Table I). These values are shown as bold arrows above the PL spectra in Fig. 2. This time the agreement with the PL data is much better: we find three exciton shells, and energies agree to within 30–40 meV. The calculated energies are consistently higher than the centers of the Gaussians fit to the PL. Part of this discrepancy is due to exchange and correlation effects between excitons in these highly excited dots (neglected in our calculations). Pseudopotential calculations with configuration interaction for multiexcitons in similar SK dots[48] predict redshifts between 5 and 30 meV due to multiexciton interactions.

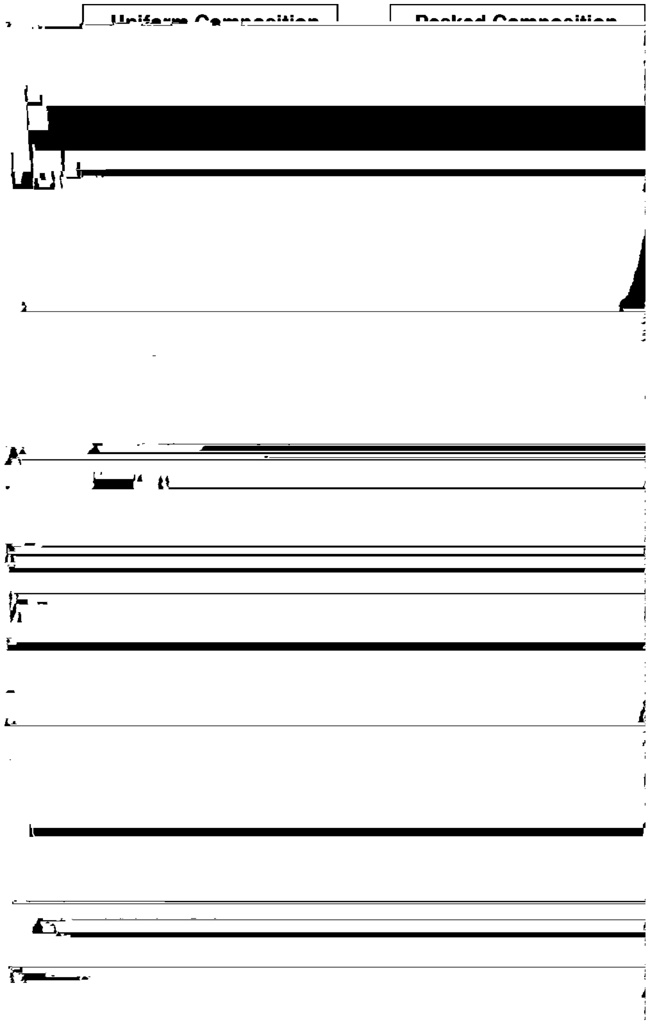

FIG. 6. Strain profiles (top) and confinement (bottom) for a dot with the geometry shown in Fig. 1(b). Left side of the figure shows results for a uniform In composition within the dot, and the right side is for nonuniform In composition, peaked in the center of the dot (t5 /(REVIEWd)-1pe6(B(a08.5(72.8338.4)-3ent)]TJ 64F5 1 Tf 2.833810 Tment)]TJ/F125302F5 1 17 25(d 7s)8889

composition (shown on the left and right sides of the figure, respectively). The jagged features in the graphs arise from atomic scale material fluctuations in the random alloy. (Such alloy fluctuations are related to exciton localization in bulk films.[17,18]) For the figure we have averaged over 72 adjacent atoms in each monolayer to reduce the fluctuations. The figure shows the strain perpendicular (ϵ_{xx}) and parallel (ϵ_{zz}) to the growth direction as well as the volume distortion (Tr ϵ). Due to the periodic boundary conditions in our calculation, there is a small coupling between vertically stacked periodic images, causing an artificial, small (<0.005), constant strain in ϵ_{xx} and ϵ_{zz}. Otherwise, the strain fields decay away from the dot, as expected for a zero-dimensional structure. We see that both the wetting layer and the dot are epitaxially strained: there is compression in the growth plane ($\varepsilon_{xx}<0$) and expansion in the growth direction ($\varepsilon_{zz}>0$). The expansion in the growth direction is compensated for by compression in the GaAs above and below the dot. Strain is considerably stronger within the dot than in the wetting layer. This is consistent with the different average In compositions, 30 and 60%, for the wetting layer and dot, respectively. For the nonuniform, peaked distribution we see a peak in the strain corresponding to the peak in the In concentration.

To illustrate the effect of strain and composition on confinement properties, we have calculated the strain-modified confinement potentials using a simple $\mathbf{k}\cdot\mathbf{p}$ model describing the coupling of harmonic strain to the valence-band maximum and conduction-band minimum of cubic materials.[53] This approximation is not a necessary step to our calculations, since these modeled confinements never enter the pseudopotential calculations. Rather, the confinement potentials are a useful tool for giving a qualitative picture of the confinement mechanism. The confinement potentials for electrons, heavy holes, and light holes are shown in the bottom part of Fig. 6. The left side of the figure shows the confinement potential for uniform composition, and the right side of the figure shows the effects of a nonuniform, peaked In distribution on the confinement potential. Short lines in the dot layer indicate the pseudopotential calculated electron and hole energies and arrows denote the thresholds of the wetting layer continua for electrons and holes. From the graphs, we see that the confinement potentials resemble the strain fields for electrons and heavy holes, while the light hole potential is relatively flat. Due to the weak light hole confinement, we expect bound hole states to be predominately heavy hole in nature. The confinement of the electrons and heavy holes is much stronger in the dot than the wetting layer, and the dot with nonuniform, peaked composition has a peaked confinement potential, too. Thus we see a trend for stronger confinement with increasing In content (as a result of the smaller band gap of InAs, even in the presence of larger strain), and might expect our pseudopotential calculations to show stronger electron and heavy hole binding with either increasing In content or nonuniform, peaked compositions.

C. Pseudopotential results for uniform composition

Using the pseudopotential method, we have calculated single-particle energies, Coulomb matrix elements, and exciton energies for Model 2 dots with a uniform composition profile and $\overline{x}_{\mathrm{In}}=50$, 55, and 60%. Figure 7 shows the change in single-particle energies as the In content is increased but kept uniform. For the range of In concentration considered, the binding energy of electrons and holes increases nearly linearly with increasing In content. In going from $\overline{x}_{\mathrm{In}}=50\%$ to $\overline{x}_{\mathrm{In}}=60\%$, the electron energies change by about 35 meV, and the hole energies change by about 20 meV. Thus our expectation based on the strain-modified confinement potentials are born out.

Two mechanisms cause the exciton energy to be red-shifted when the In content increases: (i) the electron and hole become more tightly bound to the dot, which decreases the difference in single-particle energies $\Delta\varepsilon$, and (ii) the located near 1.315 eV associated with a third exciton shell $e_3 - h_3$, $e_{4\,h}$

[39] S. Malik, C. Roberts, R. Murray, and M. Pate, Appl. Phys. Lett. **71**, 1987 (1997).

[40] S.J. Xu, X.C. Wang, S.J. Chua, C.H. Wang, W.J. Fan, J. Jiang, and X.G. Xie, Appl. Phys. Lett. **72**, 3335 (1998).

[41] S. Fafard and C.N. Allen, Appl. Phys. Lett. **75**, 2374 (1999).

[42] B. Lita, R.S. Goldman, J.D. Phillips, and P.K. Bhattacharya, Appl. Phys. Lett. **75**, 2797 (1999).

[43] R. Leon, D.R.M. Williams, J. Krueger, E.R. Weber, and M.R. Melloch, Phys. Rev. B **56**, R4336 (1997).

[44] N. Perret, D. Morris, L. Franchomme-Fossé, R. Côté, S. Fafard, V. Aimez, and J. Beauvais, Phys. Rev. B **62**, 5092 (2000).

[45] M. DeGiorgi, A. Vasanelli, R. Rinaldi, M. Anni, M. Lomascolo, S. Antonaci, A. Passeseo, R. Cingolani, A. Taurino, M. Catalno, and E. DiFabrizio, Micron **31**, 245 (2000).

[46] Note that standard envelope function calculations of the wetting layers make a number of approximationa, not shared by pseudopotential methods, e.g., the virtual crystal approximations, use of harmonic elasticity even for large lattice mismatches, and approximate electron-hole Coulomb energies. These differences lead to different electronic structure. A comparison of eight band $\mathbf{k}\cdot\mathbf{p}$ and pseudopotential calculations for quantum wells superlattices is given by D.M. Wood and A. Zunger, Phys. Rev. B **53**, 7949 (1996), showing that for $\lesssim 4$-ML thick structures the errors of $\mathbf{k}\cdot\mathbf{p}$ are indeed significant.

[47] A. Franceschetti, H. Fu, L.W. Wang, and A. Zunger, Phys. Rev. B **60**, 1819 (1999).

[48] A.J. Williamson, A. Franceschetti, and A. Zunger, Europhys. Lett. **53**, 59 (2001).

[49] P.N. Keating, Phys. Rev. **145**, 637 (1966).

[50] R.M. Martin, Phys. Rev. B **1**, 4005 (1970).

[51] A. Silverman, A. Zunger, R. Kalish, and J. Adler, Phys. Rev. B **51**, 10 795 (1995).

[52] W. Yang, H. Lee, T.J. Johnson, P.C. Sercel, and A.G. Norman, Phys. Rev. B **61**, 2784 (2000).

[53] S.-H. Wei and A. Zunger, Phys. Rev. B **49**, 14 337 (1994).